Beyond Vinyl: Electronic Structure of Unsaturated Propen-1-yl, Propen-2-yl, 1-Buten-2-yl, and *trans*-2-Buten-2-yl Hydrocarbon Radicals

Lucas Koziol, Sergey V. Levchenko, and Anna I. Krylov*

Department of Chemistry, University of Southern California, Los Angeles, California 90089-0482

Received: September 21, 2005; In Final Form: November 10, 2005

Vertical excitation energies and oscillator strengths for several valence and Rydberg electronic states of vinyl, propen-1-yl, propen-2-yl, 1-buten-2-yl, and *trans*-2-buten-2-yl radicals are calculated using the equation-of-motion coupled cluster methods with single and double substitutions (EOM-CCSD). The ground and the lowest excited state (n ← π) equilibrium geometries are calculated using the CCSD(T) and EOM-SF-CCSD methods, respectively, and adiabatic excitation energies for the n ← π state are reported. Systematic changes in the geometries, excitation energies, and Rydberg state quantum defects within this group of radicals are discussed.

1. Introduction

Unsaturated hydrocarbon radicals have attracted attention as reactive intermediates in hydrocarbon combustion since the late 1960s.[1−3] Similar species containing the vinyl moiety have become a versatile tool in the radical synthetic chemistry.[4] The smallest unsaturated hydrocarbon radical, vinyl, has been studied extensively both experimentally and theoretically. The ground state structure was derived by Kanamori et al. from the infrared diode laser spectra.[5] The first absorption band, with the origin at about 2.49 eV and Franck−Condon maximum near 3.08 eV, was measured in the region of 360−530 nm by visible absorption spectroscopy,[6] cavity ring-down laser absorption spectroscopy,[7,8] and action spectroscopy of the jet-cooled radicals[9] and was assigned to the $\tilde{A}^2A'' \leftarrow \tilde{X}^2A'$ (n ← π) transition. Two absorption features at 164.71 nm (7.53 eV) and 168.33 nm (7.37 eV) were detected from vacuum ultraviolet flash photolysis and were assigned to a Rydberg transition.[10] A broad and featureless absorption was observed in the region of 225−238 nm (5.21−5.51 eV) using room temperature gas-phase ultraviolet spectroscopy, with a maximum cross-section at 225 nm (5.51 eV).[11] The absorption was attributed mainly to the $\tilde{C}^2A' \leftarrow \tilde{X}^2A'$ ($\pi \leftarrow \pi^*$) excitation, with a small contribution from the $\tilde{B}^2A'' \leftarrow \tilde{X}^2A'$ ($\pi^* \leftarrow$ n) excitation, assuming a larger intensity for the former transition.[11]

No direct spectroscopic measurements of propenyl or butenyl radicals have been reported so far. Recently, Butler and co-workers found evidence that the C−Br fission, the primary channel of 2-bromo-1-butene photodissociation, produces 10−20% electronically excited 1-buten-2-yl radicals (assigned to the n ← π transition based on our preliminary calculations).[12] Similar behavior was observed for 2-chloro-2-butene.[13]

A fair number of theoretical studies on the structures and energetics of the ground and several electronically excited states of vinyl have been reported.[14−19] High level ab initio calculations of the vinyl ground state equilibrium structure were also reported by Peterson and Dunning.[20] Most of the vinyl excited state calculations were on the valence n ← π (the lowest electronic state of vinyl), π^* ← n, and π^* ← π states. Vertical excitation energies for several Rydberg transitions were calculated by Mebel et al.,[17] although the Rydberg states were not characterized in terms of the quantum numbers, nl_m.

Unlike vinyl, propenyl and butenyl radicals have not been characterized theoretically. These radicals are derived from vinyl by substituting one or two of its hydrogen atoms with methyl or ethyl groups, and consequently, they inherit some of its properties with slight modifications. However, the substituents can also bring around some unique properties. In this work, we present accurate ab initio calculations of the ground and first excited state equilibrium structures of vinyl, propen-1-yl, propen-2-yl, 1-buten-2-yl, and *trans*-2-buten-2-yl radicals. We also present vertical excitation energies and oscillator strengths for both valence and Rydberg states, as well as permanent dipole moments for the valence states. The changes in geometries, excitation energies, and properties of the ground and excited states in the above sequence of radicals are discussed and analyzed. Moreover, a qualitative picture of the effect of methyl or ethyl group substitutions on the electronic properties is derived to provide a basis for understanding the effects of molecular size and structure on the Rydberg states' quantum defect. In addition, we present new and interesting examples of hyperconjugation in hydrocarbons.

The paper is organized as follows. Section 2.1 summarizes the technical details of the calculations. Section 2.2 presents the analysis of the ground state equilibrium geometries of the radicals. The calculated vertical electronic spectra are discussed in section 2.3. In sections 2.4, 2.6, 3, and 4, the changes in the excitation energies and properties for different groups of excited states are discussed for the vinyl → propen-1-yl → propen-2-yl → *trans*-2-buten-2-yl → 1-buten-2-yl sequence. Section 2.5 presents adiabatic excitation energies and optimized geometries, as well as their changes in the above sequence for the lowest excited $^2A'' \leftarrow {}^2A'$ (n ← π) state. Finally, section 5 summarizes our conclusions.

2. Results and Discussion

2.1. Computational Details. The equilibrium ground state geometries were optimized by CCSD(T)[21,22] using the ACES II electronic structure program.[23] The restricted open-shell Hartree−Fock (ROHF) doublet reference was used in all the optimizations. We employed the 6-311(2+,2+)G(d,p) basis to calculate the equilibrium structures of vinyl, propen-1-yl, and propen-2-yl, and the 6-311(+,+)G(d,p) basis for 1-buten-2-yl

10.1021/jp055375r CCC: $33.50
Published on Web 02/04/2006

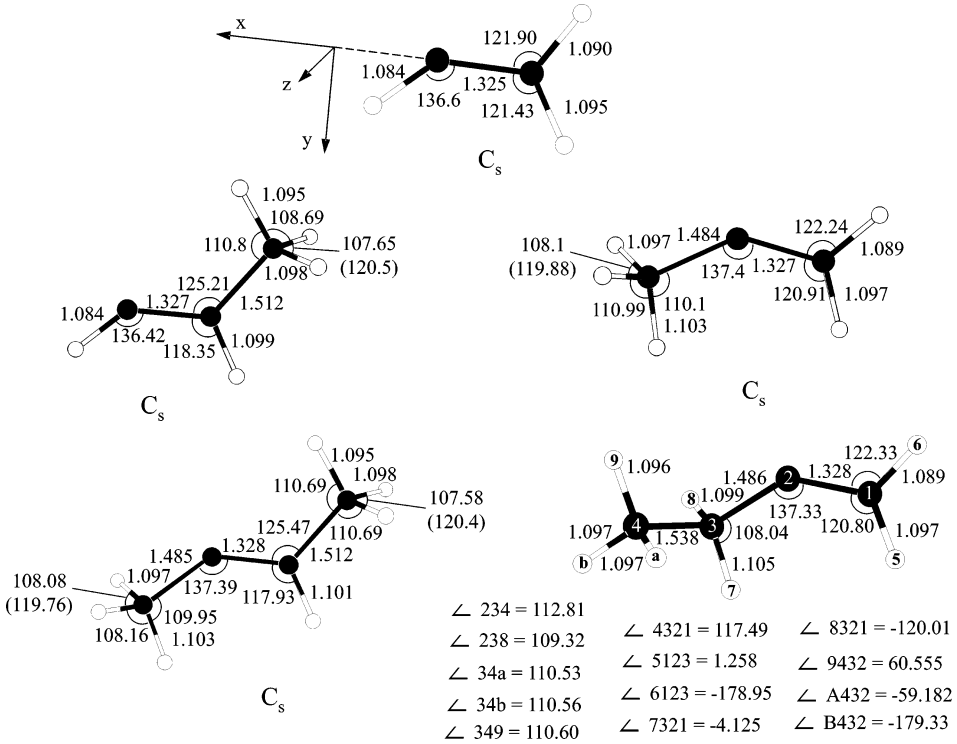

Figure 1. The CCSD(T)/6-311(2+,2+)G(d,p) ground state optimized geometries of the vinyl, propenyl, and butenyl radicals, and the molecular orientation in the Cartesian coordinate system. For 1-buten-2-yl, the *OXY* plane is the $C_1C_2C_3$ plane.

and *trans*-2-buten-2-yl. The bases were derived from the polarized split-valence 6-311G(d,p) basis[24,25] by augmenting it with additional sets of diffuse functions. Pure angular momentum spherical harmonics (5 d-functions) were used throughout this study. As shown in Figure 1, all of the radicals except 1-buten-2-yl have C_s symmetry.

Relevant molecular orbitals are shown in Figure 2. In this notation, the ground state electronic configuration is $(\pi)^2(n)^1$. The vertical excitation energies are calculated using the EOM-EE-CCSD method[26,27] with the ROHF $(\pi)^2(n)^1$ doublet reference, except for the $\pi^* \leftarrow \pi$ states (one quartet and two doublets), for which the EOM-SF-CCSD method[28] with the ROHF $(\pi)^1(n)^1(\pi^*)^1$ quartet reference was used. For the $3s \leftarrow \pi$ states, additional calculations were performed using the EOM-SF-CCSD method with the ROHF $(\pi)^1(n)^1(3s)^1$ quartet reference and Hartree−Fock orbitals optimized for the ROHF doublet reference. The ionization potentials (IPs) were calculated by EOM-IP-CCSD.[29−31]

The 6-311(2+,2+)G(d,p) basis was employed for all single-point excited state calculations, as well as for the IPs for the ionization from the half-filled orbital n. The IPs for the ionization from the π bonding orbital were calculated using the 6-311++G(d,p) basis set. In the excited state calculations, four lowest and four highest molecular orbitals were frozen for the butenyl radicals, whereas all the orbitals were active for vinyl and propenyls. The permanent dipole moment for the ground and excited states was calculated using the nonrelaxed EOM-CCSD one-particle density matrix.[27,28] The ground state density matrix was calculated by the EOM-SF-CCSD method with the ROHF $(\pi)^1(n)^1(\pi^*)^1$ quartet reference.

The geometries of the lowest excited state, $n \leftarrow \pi$, were optimized using the EOM-SF-CCSD method with the unrestricted Hartree−Fock (UHF) quartet reference. The 6-311-(2+,2+)G(d,p) and 6-311(+,+)G(d,p) basis sets were used for the vinyl and propenyl radicals and for the butenyl radicals, respectively. All orbitals were active in the excited state geometry optimizations. The assignment of the valence and Rydberg character to the excited states was based on three criteria: (i) the symmetry of the transitions, (ii) the character of the molecular orbitals in the leading EOM-CCSD amplitudes,

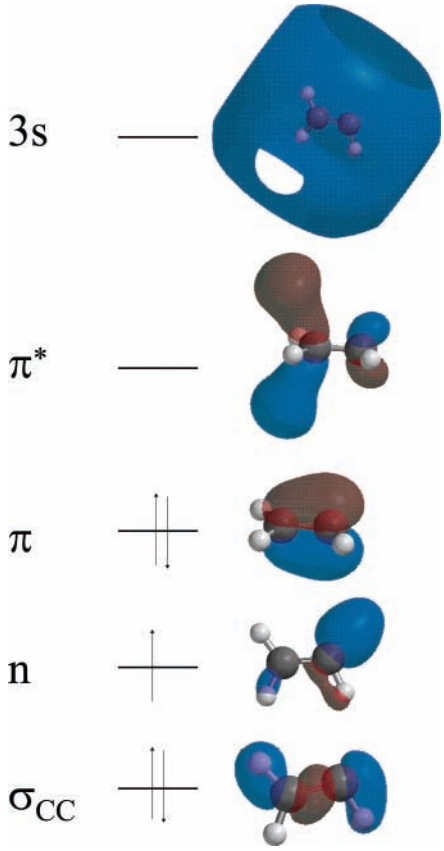

Figure 2. The σ_{CC}, π, n, π^*, and 3s ROHF orbitals of vinyl. These orbitals are very similar in all the radicals.

and (iii) the second moments, $\langle X^2 \rangle$, $\langle Y^2 \rangle$, and $\langle Z^2 \rangle$, of the EOM-CCSD electron density. All EOM calculations were performed using Q-CHEM.[32] The character of the Hartree−Fock orbitals was determined using the Spartan interface.

2.2. Ground State Equilibrium Structures. The equilibrium geometries of the vinyl, propenyl, and butenyl radicals are presented in Figure 1 (we calculated only the lowest energy, that is, trans-conformers, of the propen-1-yl and 2-buten-2-yl radicals). The common feature of all the species is the C−C double bond and the unpaired electron on one of the unsaturated sp^2-like carbon orbitals. In the subsequent discussion, we shall refer to the carbon hosting the unpaired electron as α-C, and the other unsaturated carbon atom as β-C. Atoms (groups) attached to α-C or β-C will be referred to as α-atom (α-group) or β-atom (β-group), respectively. The distance between the α- and β-carbons will be referred to as r_{CC}. The notation αCC will be used for the angle between the two σ bonds connecting α-C to other atoms.

The simplest member of this family, the vinyl radical, is derived from ethylene by removing one hydrogen atom. This results in a slight contraction of the C−C bond ($r_{CC} = 1.325$ Å in vinyl vs 1.330 Å in ethylene) and a larger αCC angle ($\angle$αCC $= 136.6°$ in vinyl vs 121.7° in ethylene). Both effects can be explained by the delocalization of the unpaired electron leading to a larger weight of the p orbital in the singly occupied sp^2 hybrid orbital on α-C, which, consequently, changes the hybridization of the other two sp^2 orbitals toward sp, with the angle closer to 180°. The H−β-C−H angle is not affected by the hydrogen removal, while the β-group is rotated as a whole toward the α-H atom in the plane of the molecule. This observation suggests that the steric repulsion between the neighboring H atoms is not the dominant factor in the αCC angle increase. This is also supported by a very weak dependence of the αCC angle on the distance between the neighboring hydrogens and by the fact that this angle is, in most cases, larger for species where the distance between the neighboring H atoms is larger.

Derived by the substitution of a β-hydrogen by a methyl group, the propen-1-yl radical exhibits only slight changes in the αCC angle and the r_{CC} distance relative to vinyl. Interestingly, whereas the angle between the β-hydrogen and the methyl group remains almost the same as that in vinyl and ethylene, the rotation of the β-group toward α-H is more pronounced in propen-1-yl than in vinyl. This implies that the rotation is due to the repulsion between the diffuse unpaired electron and the electron density localized between β-C and the attached atom or group, while the angle between the two β-hydrogens in vinyl or the β-hydrogen and the methyl group in propen-1-yl is determined by the sp^2 hybridization on β-C. The repulsion is also responsible for the small increase in r_{CC} in propen-1-yl relative to vinyl.

The propen-2-yl radical is derived by substituting the α-hydrogen of vinyl with a methyl group. A small increase (∼1°) in the αCC angle indicates an enhanced delocalization of the unpaired electron due to its repulsion from electrons localized along the C−C bonds. The delocalization leads to a slightly larger β-group rotation than in vinyl, although not as large as that in the propen-1-yl radical, where the unpaired electron interacts with more dense electronic cloud between β-C and the methyl group.

All the effects described above are found to be additive. If both α-H and β-H of vinyl are replaced with methyl groups to produce the *trans*-2-buten-2-yl radical, the value of the αCC angle approaches that of propen-2-yl, and the β-group rotates by the same number of degrees as in propen-1-yl.

The structural consequences of the substitution of the α-hydrogen from vinyl with an ethyl group, which leads to the 1-buten-2-yl radical, are very similar to those due to a methyl group in propen-2-yl, except that in 1-buten-2-yl the vinyl moiety is slightly nonplanar ($\angle 6125 = 179.79°$, according to atom numbering from Figure 1).

The equilibrium orientation of methyl groups in hydrocarbons is an interesting problem (see ref 33 for a comprehensive review). As shown by Prophristic and Goodman,[34] the major factor responsible for the staggered geometry of ethane (i.e., structure with dihedral angle HCCH = 60°) is not the steric repulsion of the C−H bonds, but rather the transfer of electrons from one methyl group to the other, leading to their participation in the C−H bonding of the other methyl group. This effect, termed hyperconjugation, stabilizes the relative orientation of the methyl groups, which maximizes the overlap of σ_{CH} bonding orbitals on one methyl group with the antibonding orbitals on the other methyl group. The mechanism of the hyperconjugative charge transfer was first suggested by Weinhold[35] and varies from one molecule to another. For example, in the propene molecule, which can be derived from both propen-1-yl and propen-2-yl radicals by adding hydrogen to the radical center, the orientation of the methyl group is the same as that in the radicals (see Figure 1). This orientation (called eclipsed in ref 33) is stabilized by participation of the σ_{CH} electrons of the two out-of-plane C−H bonds in the π bonding of the double bond (in other words, it is stabilized by the hyperconjugative charge transfer from the σ_{CH} bond of the methyl group to the π antibonding orbital of the double bond[33]). Certainly, this type of hyperconjugation plays a role in stabilizing the structures of the propenyl and *trans*-2-buten-2-yl radicals. However, there is a stronger hyperconjugative effect in the propen-2-yl and both butenyl radicals, namely, the transfer of electron density from the in-plane σ_{CH} bond to the radical center. This follows from the observation that one of the hydrogens in the ethyl group of 1-buten-2-yl is almost coplanar with the vinyl moiety, indicating that it is the overlap between the in-plane σ_{CH} bonding orbital and the partially filled lone pair of α-C that stabilizes the orientation of the ethyl group in 1-buten-2-yl. This is also confirmed by a small but systematic elongation of the in-plane σ_{CH} bond in all the propenyl and butenyl radicals. The hyperconjugation with unpaired electrons has been suggested to stabilize radical products of bond dissociation for several other molecular systems.[36] Note that the geometry of the ethyl group in 1-buten-2-yl is staggered and is very close to that of ethane.

2.3. Electronically Excited States: Vertical Spectra. The vertical excitation energies, oscillator strengths, and dipole strengths (squared transition dipole moments) for vinyl, propen-1-yl, propen-2-yl, 1-buten-2-yl, and *trans*-2-buten-2-yl are summarized in Tables 1, 2, 3, 5, and 4, respectively. The $\langle S^2 \rangle$ values are also given as a measure of reliability of the calculated energies and, especially, properties: large spin contamination indicates possible errors in the excitation energies, as well as large errors in transition strengths and permanent dipole moments. The results are also visualized in Figures 3−7 as stick spectra. Note that only singly excited states are shown. Also, since the highest $\pi^* \leftarrow \pi$ state was calculated separately from the rest, there are more states in the energy region between this state and the second-highest one shown on the pictures. The electronic spectra of the radicals at hand are very dense and

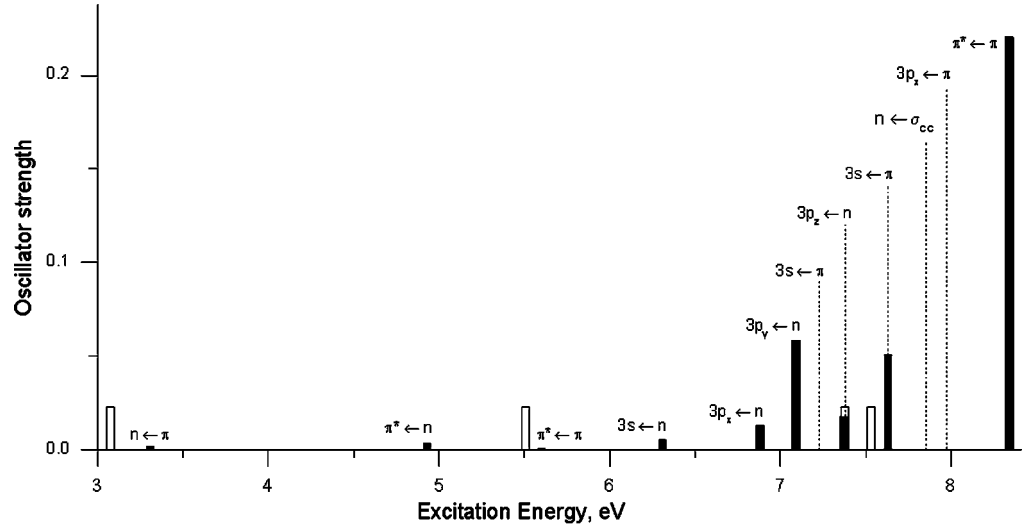

Figure 3. Calculated vertical electronic excitation energies and oscillator strengths of the vinyl radical. The reported experimental excitation energies (see Introduction for references) are shown by hollow bars. The intensity of the experimental transitions is arbitrary.

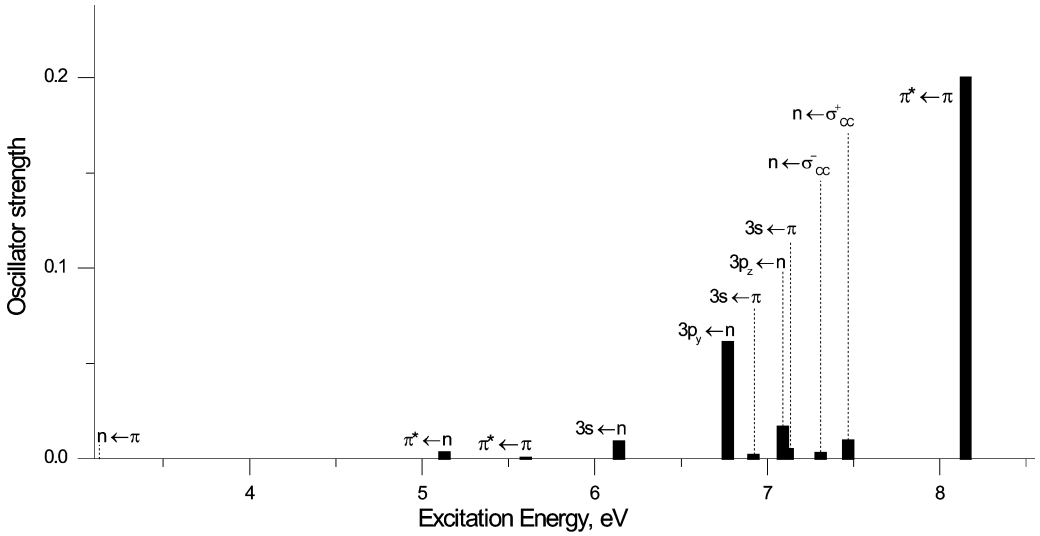

Figure 4. Calculated vertical electronic excitation energies and oscillator strengths of propen-1-yl.

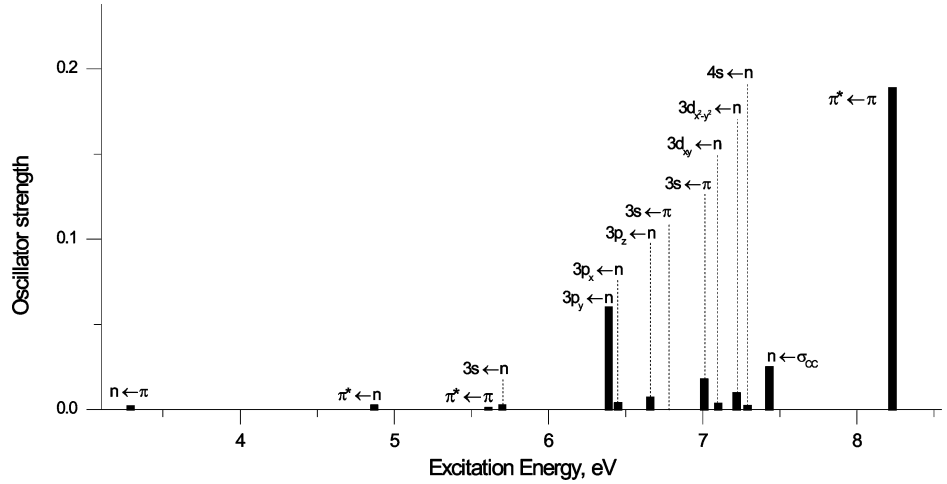

Figure 5. Calculated vertical electronic excitation energies and oscillator strengths of propen-2-yl.

are dominated by the Rydberg excitations. In the following sections, we discuss the systematic changes in excitation energies and intensities of the calculated transitions. The permanent dipole moments of the radicals in the ground and valence excited states (at the ground state equilibrium geometries) are shown in Figures 9 and 11. The ground state permanent dipole moments (in atomic units) are (0.106, −0.243, 0) for vinyl, (0.216, −0.164, 0) for propen-1-yl, (−0.110, −0.318, 0) for propen-2-yl, (−0.113, −0.309, −0.014) for 1-buten-2-yl, and (−0.001, −0.246, 0) for *trans*-2-buten-2-yl.

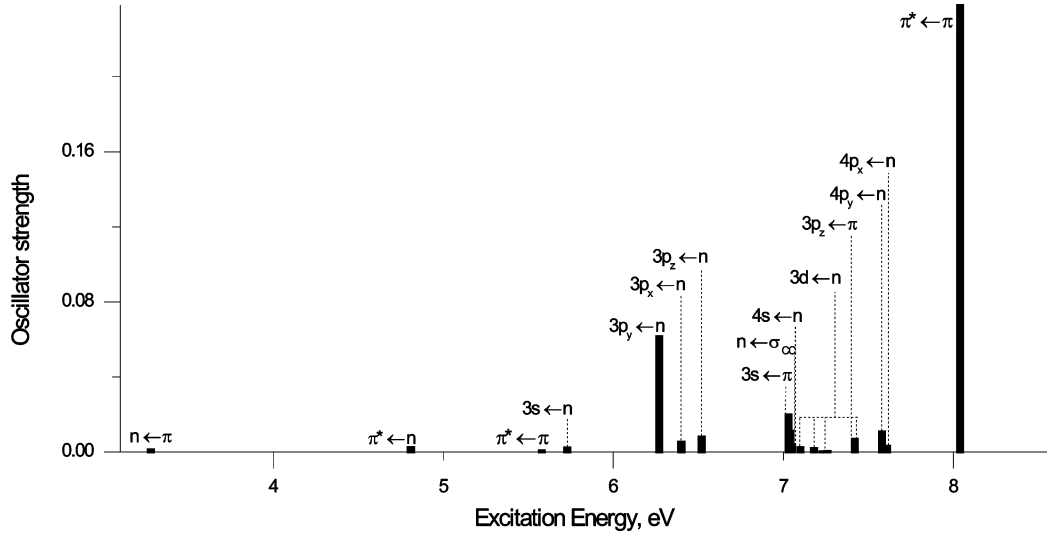

Figure 6. Calculated vertical electronic excitation energies and oscillator strengths of 1-buten-2-yl.

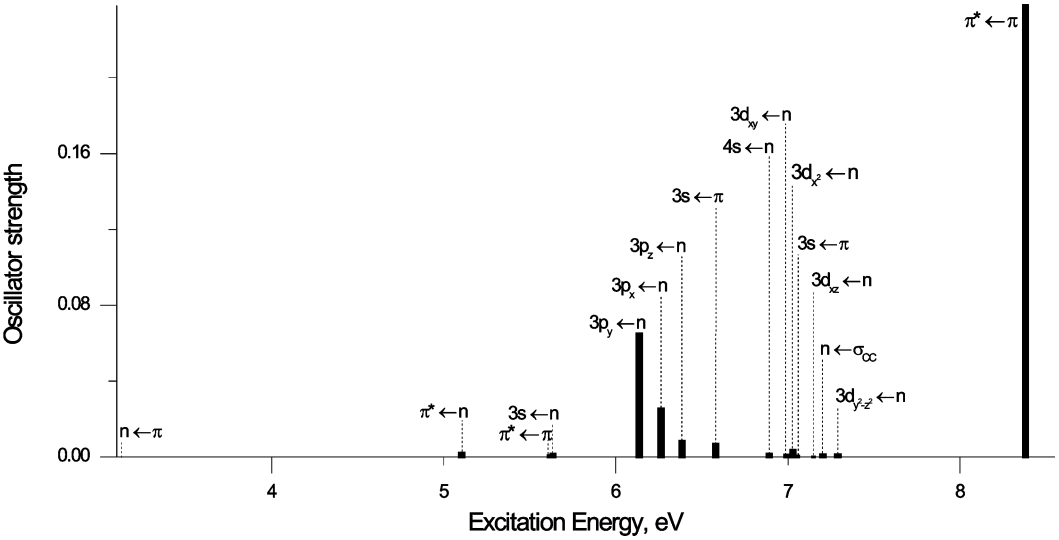

Figure 7. Calculated vertical electronic excitation energies and oscillator strengths of *trans*-2-buten-2-yl.

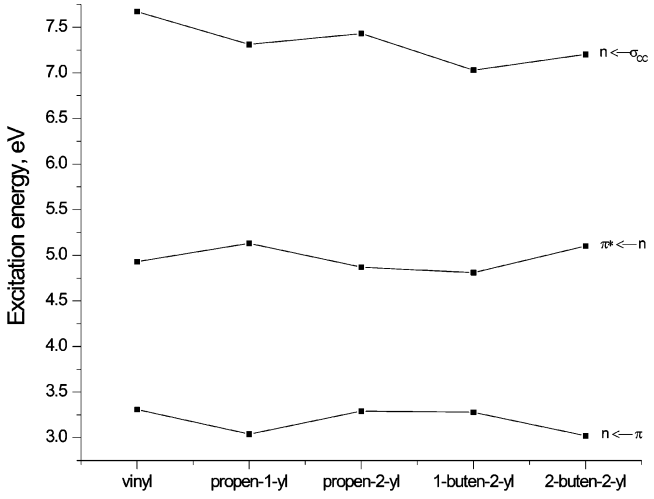

Figure 8. Changes in the n ← π, π* ← n, and n ← σ_{CC} vertical excitation energies.

It was first pointed out by Mebel et al.[17] that the two absorption features of vinyl, at 7.37 and 7.53 eV, observed by Fahr and Laufer,[10] could be due to different electronic states rather than vibrational spacing. On the basis of their calculations, Mebel et al. suggested n ← σ (excitation energy 7.31 eV) and Ryd ← π (excitation energy 7.48 eV) as candidates for these transitions. Their excitation energy for the Rydberg state is very close to our excitation energy for the 3s ← π state (7.47 eV). Our excitation energy for the n ← σ state of vinyl is larger (7.67 eV); however, we found another state, $3p_z$ ← n, at 7.38 eV, which is very close to one of the observed peaks. Moreover, this state, as well as the 3s ← π one, is much more intense than the n ← σ state. Thus, we suggest that the $3p_z$ ← n and 3s ← π states are responsible for the observed transitions.

2.4. Valence Excited States Derived from the n ← π, π* ← n, and n ← σ_{CC} Transitions. The valence excited states derived from the n ← π, π* ← n, and n ← σ_{CC} transitions do not have analogues in ethylene. These states correspond to electron promotion to or from the half-filled orbital. Thus, single excitations from the doublet reference determinant provide a spin-complete zeroth-order description of these states. Therefore, EOM-EE-CCSD describes these states accurately.[28,37]

Figure 8 shows changes in these vertical excitation energies in the vinyl → propen-1-yl → propen-2-yl → 1-buten-2-yl → *trans*-2-buten-2-yl series. The corresponding changes in the oscillator strengths and permanent dipole moments are shown in Figure 9. The n ← π state, which corresponds to the excitation from the α-C−β-C π bond to the partially filled α-C sp^2 orbital,

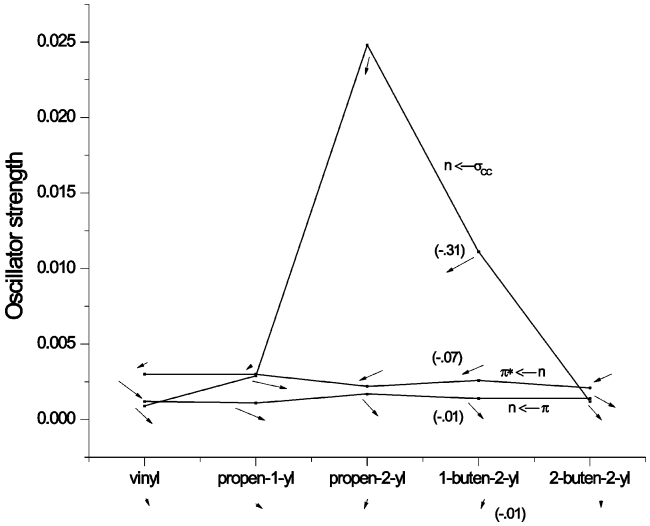

Figure 9. Changes in the oscillator strengths for the n ← π, π^* ← n, and n ← σ_{CC} transitions. The ground and vertical excited state permanent dipole moments are shown by arrows. The plane of the figure is considered as the *OXY* plane, and the *OZ* axis is perpendicular to this plane (see Figure 1). For 1-buten-2-yl, the *Z*-component of the permanent dipole moment is shown in parentheses.

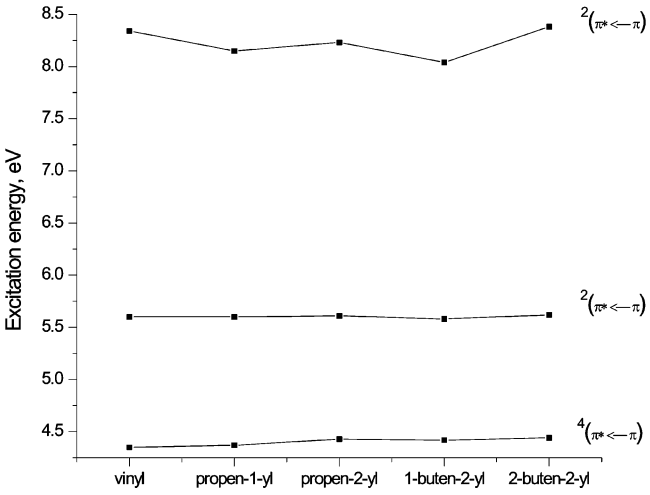

Figure 10. Changes in the π^* ← π vertical excitation energies.

is the lowest in all the radicals. The vertical excitation energy for this state is about 3.3 eV in vinyl, propen-2-yl, and 1-buten-2-yl, whereas it is lower by 0.3 eV in propen-1-yl and *trans*-2-buten-2-yl. This change is consistent with the structural differences (see Figure 1): the radicals with the same β-group have similar excitation energies, which means that it is not the change in the half-filled orbitals, rather the change in the π bonding orbitals that is responsible for the change of the excitation energy. The same holds for the π^* ← n state (see Figure 8), although the β-group substitution has an opposite effect: the vertical excitation energy is about 4.9 eV for vinyl, propen-2-yl, and 1-buten-2-yl, but it is *higher* by about 0.2 eV for propen-1-yl and *trans*-2-buten-2-yl. This can be rationalized as follows: the increase of electron density on the β-group upon the substitution of hydrogen with a methyl group causes the energies of the π and π^* orbitals to increase, while at the same time having minor relative effect on the energy of the half-filled orbital. Consequently, it becomes easier to move an electron from the π orbital to n, but harder to excite an electron from n to π^*. Moreover, the energy gap between the π and π^* orbitals is not affected by the substitution, as follows from the

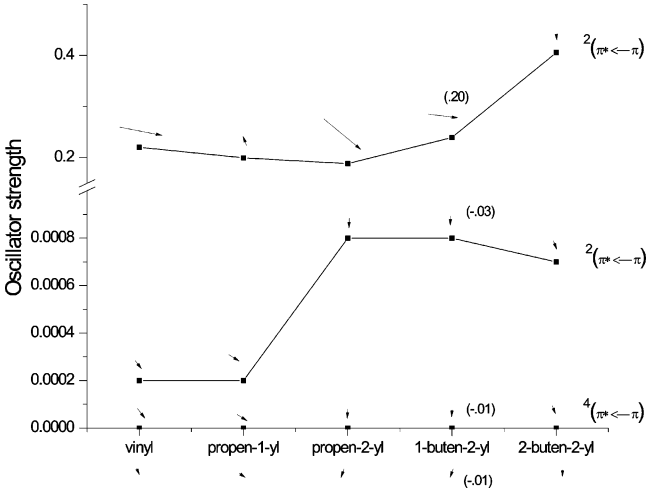

Figure 11. Changes in the oscillator strengths for the π^* ← π transitions. The ground and vertical excited state permanent dipole moments are shown by arrows. The plane of the figure is considered as the *OXY* plane, and the *OZ* axis is perpendicular to this plane (see Figure 1). For 1-buten-2-yl, the *Z*-component of the permanent dipole moment is shown in parentheses.

structural insensitivity of the first π^* ← π doublet vertical excitation energy (see Figure 10).

The changes in the n ← σ_{CC} excitation energies are more complicated. There are as many different n ← σ_{CC} states as there are different σ_{CC} bonds. The molecular orbital and the EOM-CCSD amplitude analyses reveal that the different σ_{CC} bonds form a delocalized σ_{CC} system, from which the excitation occurs. Finally, the n ← σ_{CC} states are fairly high in energy (above 7 eV), where the density of states is high, and they mix with the Rydberg states of the same symmetry. This explains why some of the n ← σ_{CC} states are missing, such as n ← σ_{CC}^+ for the propen-2-yl radical. There are two n ← σ_{CC} transitions in propen-1-yl: at 7.31 eV (n ← σ_{CC}^-) and 7.47 eV (n ← σ_{CC}^+), with both of them being lower than the n ← σ_{CC} transition in vinyl (7.67 eV). We interpret this in terms of reduced repulsion between the σ_{CC} bonds, due to removal of an electron from one of the bonds. Alternatively, one can picture the resulting positive σ_{CC} system as being stabilized by the higher number of bonds in the system, analogous to the decreasing basicity of amines in the order tertiary, secondary, and primary. The two methods are equivalent in explaining the observed trend of decreasing n ← σ_{CC} excitation energies with increasing number of σ_{CC} bonds (see Figure 8).

Despite the delocalization of the n ← σ_{CC} excitations in propen-1-yl, we can assign, based on the values of the dipole strengths, the n ← σ_{CC}^- transition at 7.31 eV as an excitation from the σ_{CC} bond between α-C and β-C (lower transition strength, the electron is transferred to n from the closer bond), whereas the n ← σ_{CC}^+ transition at 7.47 eV is from the σ_{CC} bond between β-C and the carbon atom of the methyl group (higher transition strength, the charge is transferred over larger distance). This is also consistent with changes in the permanent dipole moment upon excitation (see Figure 9).

The higher excitation energy for the n ← σ_{CC}^- transition in propen-2-yl (7.43 vs 7.31 in propen-1-yl) is due to increased repulsion between the additional electron on the half-filled orbital and the electrons participating in the carbon σ bonding. The excitation occurs mainly from the longer C−C bond; the electrons from the C−H bonds of the methyl group compensate for the decrease in electron density between the carbons due to high polarizability of the C−H bonds. This electron transfer

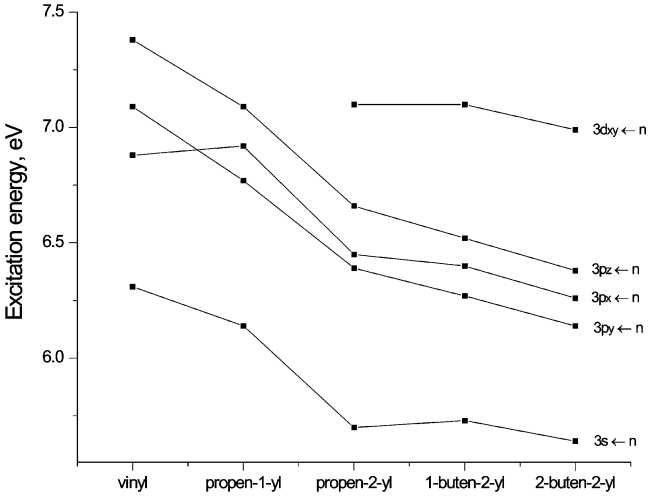

Figure 12. Changes in the $nl_m \leftarrow n$ vertical excitation energies.

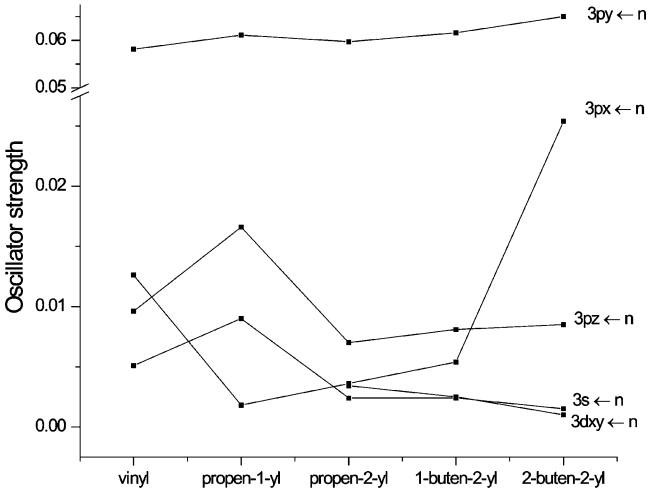

Figure 13. Changes in the oscillator strengths for the $nl_m \leftarrow n$ transitions. The ground and vertical excited state permanent dipole moments are shown by arrows. The plane of the figure is considered as the *OXY* plane, and the *OZ* axis is perpendicular to this plane (see Figure 1). For 1-buten-2-yl, the *Z*-component of the permanent dipole moment is shown in parentheses.

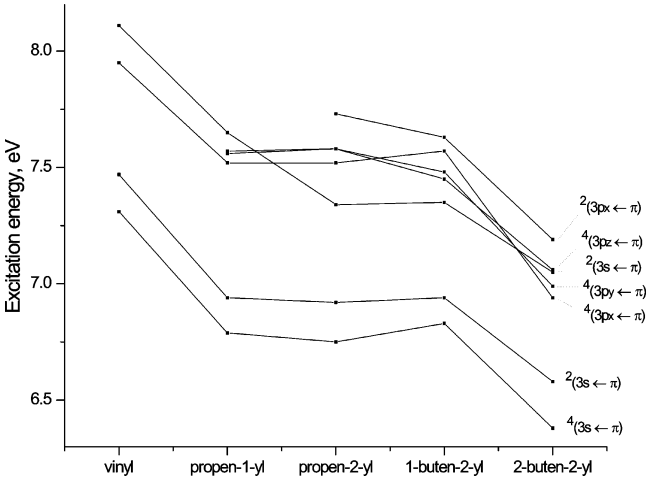

Figure 14. Changes in the $nl_m \leftarrow \pi$ vertical excitation energies.

explains the high oscillator strength for the $n \leftarrow \sigma_{CC}^-$ transition in propen-2-yl (see Figure 9).

In *trans*-2-buten-2-yl and 1-buten-2-yl, the increased number of σ_{CC} bonds relative to propen-1-yl and propen-2-yl results in increased repulsion between the electrons forming these bonds and, consequently, in the decrease of the $n \leftarrow \sigma_{CC}$ excitation energies. The lowest $n \leftarrow \sigma_{CC}^-$ excitation in *trans*-2-buten-2-yl corresponds mainly to the excitation from the double bond. The positive charge created is farther from the methyl hydrogens, which results in a decreased electron donation from the methyl groups and consequent lower oscillator strength relative to propen-2-yl. Due to the lower symmetry, the $n \leftarrow \sigma_{CC}$ and $3s \leftarrow \pi$ states are allowed to mix in the 1-buten-2-yl radical. The EOM-CCSD amplitude analysis supports this interpretation. The driving force for this mixing is the increase of the repulsion between the lone pair on α-C and the π bond upon the $n \leftarrow \sigma_{CC}$ excitation. The possibility to remove an electron from the π bond provides an additional degree of freedom for relaxation, which explains the lower excitation energy for the $n \leftarrow \sigma_{CC}$ transition in 1-buten-2-yl (7.03 eV) relative to *trans*-2-buten-2-yl (7.20 eV).

2.5. Equilibrium Geometries and Adiabatic Excitation Energies for the $n \leftarrow \pi$ Excited States. Equilibrium geometries of the $n \leftarrow \pi$ states are summarized in Figure 15. The most prominent change in the geometric parameters upon the $n \leftarrow \pi$ excitation is the elongation of the α-C−β-C bond and the decrease of the αCC angle. The elongation of the C−C bond is, of course, due to the decrease in the bond order from 2 (one σ and one π bond) to 1.5 (one σ and half of a π bond). The decrease of the αCC angle is due to the decreased delocalization of the lone pair on α-C, plus the repulsion between the lone pair and the bonds connecting α-C with neighboring atoms. Because of the decrease of the αCC angle, the steric repulsion between the α- and β-hydrogens becomes competitive with the repulsion between the lone pair on α-C and the closest bonds in the β-group, resulting in the opposite rotation of the β-group with respect to the ground state (see section 2.2). The αCC angle in propen-2-yl, 1-buten-2-yl, and *trans*-2-buten-2-yl is about 5° larger than that in vinyl and propen-1-yl due to the repulsion of the C−C bonds. These changes in the equilibrium geometries and bond angles are much larger than the error bars for the CCSD and CCSD(T) methods.[38] Changes discussed below are comparable to the systematic and nonsystematic errors of CCSD vs CCSD(T) and, therefore, should be taken with a grain of caution.

An interesting consequence of the partial breaking of the π bond upon the $n \leftarrow \pi$ excitation is the increase of electron donation from the out-of-plane C−H bonds to the α-C−β-C π bond, leading to the shortening of the α-C−β-C bond in the vinyl → propen-2-yl → 1-buten-2-yl → propen-1-yl → *trans*-2-buten-2-yl sequence. This is confirmed by the increase of the out-of-plane C−H bond lengths relative to the ground state. Although the elongation of the C−H bonds is very small (∼0.002 Å), it is likely not due to the difference between the methods used to optimize excited and ground state structures because the bonds are *elongated*, while CCSD systematically *underestimates* bond lengths relative to CCSD(T).[38] The maximum of error distribution of CCSD is shifted toward shorter bond lengths relative to CCSD(T). Also, since the excited electron is partially transferred from β-C to α-C, the C−C bond in the β-group of propen-1-yl and *trans*-2-buten-2-yl is shortened by about 0.02 Å by the excitation. The α-C−H bond in propen-1-yl and the C−C bond in the α-group of propen-2-yl, *trans*-2-buten-2-yl, and 1-buten-2-yl are elongated by ∼0.01−0.02 Å relative to the ground state because the orbitals of α-C become more sp^3-like hybridized, and the contribution of the 2s orbital to the α-C−H or α-C−C bond decreases.

The equilibrium geometry of the 1-buten-2-yl radical in the $n \leftarrow \pi$ excited state is slightly nonplanar (dihedral angle C_4−

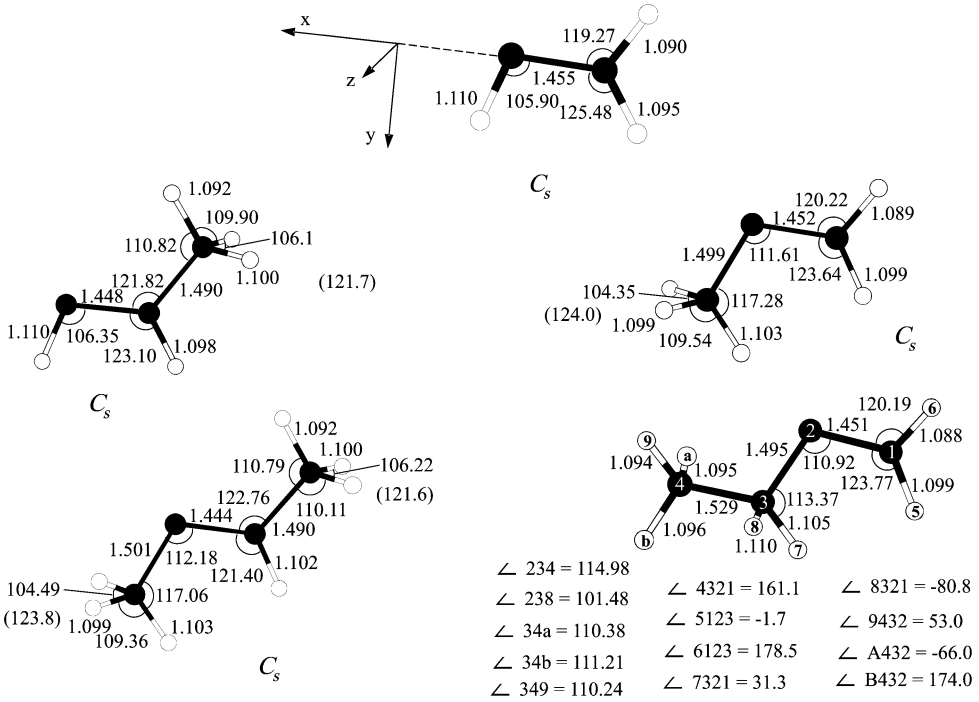

Figure 15. The EOM-SF-CCSD lowest excited state (n ← π) optimized geometries of the vinyl, propenyl, and butenyl radicals, and the molecular orientation in Cartesian coordinate system. For 1-buten-2-yl, the *OXY* plane is the $C_1C_2C_3$ plane.

$C_3-C_2-C_1$ is 161°). The calculated energy difference between the optimized planar and nonplanar structures is very small (82 cm^{-1}). We explain the small energy increase for the planar structure by the increased repulsion between the lone pair on α-C and the σ-C−C bond of the ethyl group.

The n ← π adiabatic excitation energies for the vinyl, propen-1-yl, propen-2-yl, *trans*-2-buten-2-yl, and 1-buten-2-yl radicals are 2.47, 2.24, 2.39, 2.14, and 2.33 eV, respectively. The calculated adiabatic excitation energy of vinyl, 2.47 eV, is very close to the observed origin of the lowest electronic transition, 2.49 eV.[6−8] Note that while the vertical excitation energies for the n ← π transition decrease very slowly within the vinyl → propen-2-yl → 1-buten-2-yl and propen-1-yl → *trans*-2-buten-2-yl groups (see section 2.4 and Figure 8) the adiabatic excitation energies decrease faster within these two groups (0.06−0.1 eV adiabatic vs 0.01−0.02 eV vertical excitation energy difference between the neighboring radicals in the groups). The steeper decrease of the adiabatic excitation energies is due to the increase of the number of degrees of freedom with the system size, which facilitates the relaxation of the excited state.

2.6. Excited π^* ← π States. Unlike the transitions described in section 2.4, the π^* ← π excitation is present in ethylene, where it yields two states: the triplet $^3B_{3u}$ state at 4.49 eV and the singlet $^1B_{3u}$ state at 8.18 eV vertically.[39] Due to the unpaired electron, there are *three* π^* ← π states in the radicals: one (low-spin) quartet and two doublets. The spin-pure zeroth-order wave functions of these states are[38]

$$^4\Psi = (\alpha\pi)(\alpha n)(\beta\pi^*) + (\alpha\pi)(\beta n)(\alpha\pi^*) + (\beta\pi)(\alpha n)(\alpha\pi^*)$$

$$^2\Psi_1 = 2(\alpha\pi)(\beta n)(\alpha\pi^*) - (\beta\pi)(\alpha n)(\alpha\pi^*) - (\alpha\pi)(\alpha n)(\beta\pi^*)$$

$$^2\Psi_2 = (\beta\pi)(\alpha n)(\alpha\pi^*) - (\alpha\pi)(\alpha n)(\beta\pi^*) \qquad (1)$$

It is easy to see that some of the above configurations are formally double excitations from the doublet $(\pi)^2(n)$ reference, which results in a large spin contamination of the EOM-EE-CCSD target states. The large spin contamination can cause large errors in excitation energies[40] and, especially, in oscillator strengths and permanent dipole moments. On the other hand, all of the above configurations are single spin-flipping excitations from the quartet $(\alpha\pi)(\alpha n)(\alpha\pi^*)$ reference and can be described by EOM-SF-CCSD. Consequently, the spin contamination of the EOM-SF-CCSD target states is much smaller.

The systematic changes in vertical excitation energies and properties of the π^* ← π states are summarized in Figures 10 and 11. The excitation energies for the quartet state of vinyl and propen-1-yl are very close (4.35 and 4.37 eV, respectively). The same is true for the propen-2-yl, 1-buten-2-yl, and *trans*-2-buten-2-yl radicals (4.43, 4.42, and 4.44 eV, respectively). However, the differences in excitation energy for the radicals from these two groups are larger; that is, it is at least 0.05 eV higher for propen-2-yl and both buten-2-yl isomers. We attribute this difference to the more diffuse character of the unpaired electron in the propen-2-yl and buten-2-yl isomers (confirmed by the geometry change mentioned in section 2.2), which results in a stronger Pauli repulsion for the quartet state. Indeed, this effect is observed only for the quartet π^* ← π state, for which the Pauli repulsion is stronger, while the transition energy for the first doublet is almost the same for all the radicals. The reason for the excitation energies to the quartet state for the radicals being lower than the corresponding excitation energy in ethylene is the better overlap of the carbon out-of-plane p orbitals in ethylene, due to higher symmetry.

As shown by Mulliken,[41] the transitions from a bonding orbital to the corresponding antibonding orbital are usually very strong. However, the oscillator strength of the π^* ← π transition to the first doublet in the radicals is weak (<0.001). The origin of this was first explained by Zhang and Morokuma for the vinyl radical.[18] In the lower energy doublet of vinyl, the unpaired electron is coupled to the spin-forbidden "triplet" π^* ← π configuration. However, in the second doublet, the unpaired electron is coupled to the "singlet" π^* ← π configuration, and

TABLE 1: Vertical Excitation Energies, Oscillator Strengths, and Properties of the Excited States of the Vinyl Radical[a]

state	transition	ΔE, eV	f_L	μ_{tr}^2	$\langle S^2 \rangle$
$^2A''$	$n \leftarrow \pi$	3.31	0.0012	0.0144	0.75
$^4A'$ [b]	$\pi^* \leftarrow \pi$	4.35	0	0	3.75
$^2A''$	$\pi^* \leftarrow n$	4.93	0.0030	0.0250	0.76
$^2A'$ [b]	$\pi^* \leftarrow \pi^d$	5.60	0.0002	0.0011	0.75
$^2A'$	$3s \leftarrow n$	6.31	0.0051	0.0327	0.76
$^2A'$	$3p_x \leftarrow n$	6.88	0.0126	0.0748	0.76
$^2A'$	$3p_y \leftarrow n$	7.09	0.0581	0.3346	0.76
$^4A''$ [c]	$3s \leftarrow \pi$	7.31 (7.33)	0	0	3.75
$^2A''$	$3p_z \leftarrow n$	7.38	0.0096	0.0534	0.81
$^2A''$ [c]	$3s \leftarrow \pi^e$	7.47 (7.63)	0.0594	0.3247	0.76
$^2A''$ [c]	$3s \leftarrow \pi^f$	8.11	0.0249	0.1255	0.82
$^2A'$	$n \leftarrow \sigma_{CC}$	7.67	0.0009	0.0046	0.83
$^4A''$	$3p_x \leftarrow \pi$	7.95	0	0	2.20
$^2A'$ [b]	$\pi^* \leftarrow \pi^g$	8.34	0.2204	1.0782	1.10

[a] EOM-CCSD/6-311(2+,2+)G(d,p) level of theory using ROHF doublet reference at the geometry from Figure 1 (spherical d-functions, $E_{HF} = -77.403554$ hartree). [b] Calculated by EOM-SF-CCSD with the ROHF $(\pi)^1(\pi^*)^1(n)^1$ quartet reference (spherical d-functions, $E_{HF} = -77.287220$ hartree). [c] Calculated by EOM-SF-CCSD with the ROHF $(\pi)^1(n)^1(3s)^1$ reference (orbitals are optimized for the doublet reference, the 3s orbital is the 16th α-spin orbital by energy in the Hartree−Fock ROHF doublet reference). The EOM-EE-CCSD excitation energy is shown in parentheses. [d] $2(\alpha\pi)(\beta n)(\alpha\pi^*) - (\beta\pi)(\alpha n)(\alpha\pi^*) - (\alpha\pi)(\alpha n)(\beta\pi^*)$. [e] $(\beta\pi)(\alpha n)(\alpha 3s) - (\alpha\pi)(\alpha n)(\beta 3s)$. [f] $2(\alpha\pi)(\beta n)(\alpha 3s) - (\beta\pi)(\alpha n)(\alpha 3s) - (\alpha\pi)(\alpha n)(\beta 3s)$. [g] $(\beta\pi)(\alpha n)(\alpha\pi^*) - (\alpha\pi)(\alpha n)(\beta\pi^*)$.

this transition is indeed the strongest among the calculated transitions of vinyl (see Table 1). This applies to the other species as well.

The structural dependence of the second doublet is determined by the interplay between electron repulsion and attraction of electrons to partially positive hydrogens on the methyl/ethyl groups. Indeed, due to the Coulomb repulsion between the unpaired electron and an electron on a π^* orbital in vinyl, the latter tends to be as far away from the former as possible, but it cannot go too far because of nuclear attraction. As a result, the excitation energy for the second doublet in vinyl (8.34 eV) is higher than the singlet $\pi^* \leftarrow \pi$ excitation in ethylene (8.18 eV). In propen-1-yl, the energy of the excited electron on the π^* orbital is lowered by the attraction to the out-of-plane hydrogens (see Figure 1), and the excitation energy becomes 8.15 eV, even lower than in ethylene. In propen-2-yl, in which the unpaired electron and the out-of-plane hydrogens of the methyl group are on the same side of the π bond, two trends are in opposition. Nevertheless, the energy is lowered by the attraction to the hydrogens, and the second doublet in propen-2-yl (8.23 eV) is lower than in vinyl, although it is higher than in ethylene. In 1-buten-2-yl, we have an ethyl group instead of a methyl group, and the energy of an electron on the π^* orbital is lowered even more than in propen-2-yl, resulting in a low excitation energy of 8.04 eV. Finally, in *trans*-2-buten-2-yl, the stabilizing effects of the two methyl groups lead to a less diffuse distribution of an electron on the π^* orbital, resulting in a high excitation energy of 8.38 eV, which is close to vinyl. Note that this behavior is completely different from the structural dependence of the quartet and the first doublet states because only for the second doublet are the energetics of the transition determined by Coulomb interactions rather than exchange interactions.

3. Rydberg $nl_m \leftarrow n$ States

The Rydberg $nl_m \leftarrow n$ states, which are well described by EOM-EE-CCSD, are predominantly single excitations of the unpaired electron to a diffuse Rydberg orbital. Since there are no unpaired electrons in ethylene, these excitations are unique to the radicals.

The excitation energy for the Rydberg states of small polyatomic molecules can be approximated by the Rydberg formula[42]

$$E_{ex} = IP - \frac{13.61}{(n-\delta)^2} \qquad (2)$$

where E_{ex} is the excitation energy (in eV), IP is the ionization potential of the molecule (in eV), n is the principal quantum number, and δ is the quantum defect parameter accounting for the penetration of the excited Rydberg electron to the cation core ($\delta = 0.9-1.2$ for s states, $0.3-0.6$ for p states, and smaller or equal to 0.1 for d states[42]). The ionization potential of a molecule is determined by two factors: the energy of the orbital from which the ionization occurs, and the redistribution of the electron density in the ion core upon ionization. The quantum defect δ depends on the size and the shape of a molecule. Finally, the Rydberg states can mix with valence states and other Rydberg states of the same symmetry.

The calculated IPs of vinyl, propen-1-yl, propen-2-yl, 1-buten-2-yl, and *trans*-2-buten-2-yl radicals are 9.63, 9.28, 8.79, 8.66, and 8.51 eV, respectively. The decrease of IPs in this sequence is due to increased repulsion between an unpaired electron and other electrons as the number of electrons increases. This explains the monotonic decrease (except the $3p_x \leftarrow n$ state in propen-1-yl, which is discussed below) of the excitation energies for the $nl_m \leftarrow n$ Rydberg states in the above sequence, as well as a larger decrease upon the vinyl α-hydrogen substitution compared to a β-hydrogen substitution (i.e., propen-2-yl vs propen-1-yl and propen-1-yl vs *trans*-2-buten-2-yl), as shown in Figure 12.

However, the excitation energies for Rydberg states of many-electron systems are also influenced by the interaction of the excited electron with the cation core. The strength of this interaction is characterized by the quantum defect, δ. Despite the repulsion of the valence electrons, there is a nonvanishing probability to find a Rydberg electron in such proximity to a heavy nucleus that it "feels" its higher positive charge, resulting in a positive δ in eq 2. Figure 16 presents the summary of the quantum defects for the 3s and the three components of the 3p Rydberg states of vinyl, propenyl, and butenyl radicals, along with the changes in IPs and the excitation energies upon substitution of hydrogens with methyl (ethyl in the case of 1-buten-2-yl) groups. The general trend is that the quantum defect decreases as the system size increases, which leads to a slower excitation energy drop relative to the drop in IP. This is due to the increase in the number of electrons, which screen the nuclei in the cation core.

The most intriguing result is the very large (0.76 vs 0.69 in CH_3, calculated at the same level) quantum defect for the $3p_x$ (directed along the C−C bond) Rydberg state of vinyl and its sharp drop in propen-1-yl and propen-2-yl (by about 0.16), which, as mentioned above, leads to the increased excitation energy for the propen-1-yl despite the decrease in IP. The NBO analysis[43] of the electron density for the $3p_x$ state reveals a large weight of carbon 2s orbitals in the Rydberg orbital (occupied by the excited electron) in vinyl, but not in propen-1-yl and propen-2-yl.

We did not observe any substantial mixing of the valence and the 3s or 3p Rydberg states, which would manifest itself in excitations shared by two or more EOM-CCSD target states. This does not exclude, of course, the Rydberg−valence interac-

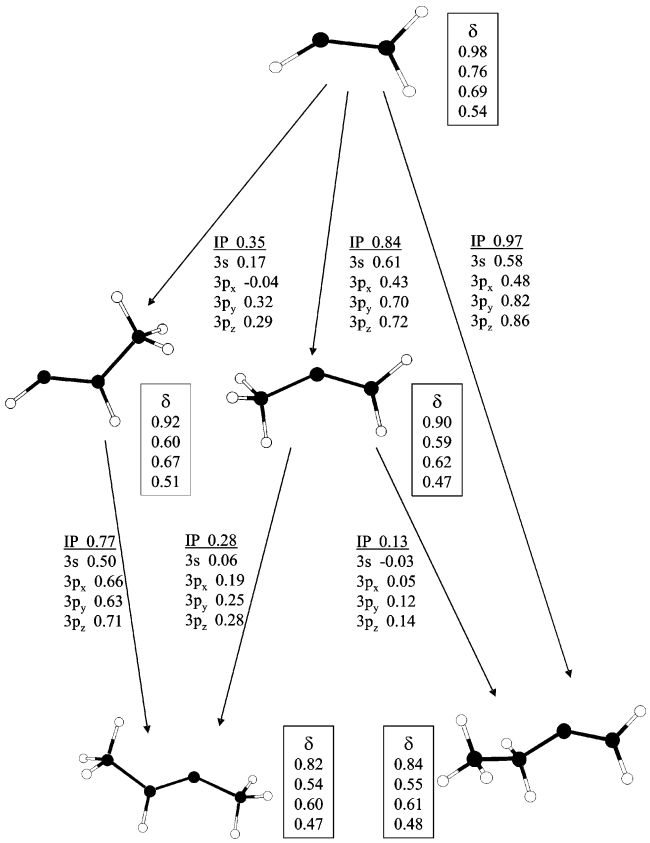

Figure 16. Quantum defects, δ, for the $nl_m \leftarrow n$ Rydberg states; see eq 2. Arrows connect species that are different by a single substitution of a hydrogen by a methyl or ethyl group. Next to the arrows, the differences in IPs, as well as in the excitation energies for the 3s, $3p_x$, $3p_y$, and $3p_z$ states (from top to bottom) for the connected species are shown.

tions due to the mixed Rydberg−valence character of the HF orbitals that reflects the diffuseness of the valence orbitals due to electron repulsion. Thus, we distinguish between the mixing of many-electron states and mixing of one-electron states. The large quantum defect for the $3p_x$ state of vinyl cannot be explained by mixing of the Rydberg and valence electronic states.

To understand this quantum defect, we performed NBO[43] analysis of the 3p Rydberg state electron density. We also analyzed the relevant MOs by using the Spartan interface.[32] The analysis clearly demonstrates that about one-half of the positive charge in the cation core is distributed among the hydrogens. Due to the high polarizability of the C−H bonds, the carbons effectively strip the hydrogens off the electrons, thus acquiring a negative charge. The MO analysis shows that the orientation of the in-plane $3p_{x,y}$ components in the radicals is determined by the anisotropy of the potential created by the positively charged hydrogens. This is why one of the 3p components ($3p_x$ in our notations) is directed along the line connecting the two far-most carbons in the radicals of C_s symmetry (vinyl, propenyl, and *trans*-2-buten-2-yl).

Contrary to atoms, the quantum defect in molecules depends also on the charge distribution in the cation core. To explain the role of this charge distribution, we consider two model systems: the methyl and methylene radicals. It is known[44] that the quantum defect δ for the in-plane components of the 3p Rydberg states in methyl (∼0.7) is larger than δ for the out-of-plane component (∼0.6), which is close to a free carbon atom. Large δ values for the in-plane components can be explained by the finite dimension of the molecule in the plane. Since the positive charge of the cation is distributed over a finite area, the maxima of the in-plane Rydberg electron wave function tend to approach the center of the charge distribution, which is the carbon atom, resulting in a higher probability of finding a Rydberg electron near the carbon nucleus. Note that both in-plane and out-of-plane Rydberg 3p electrons must have a node on the carbon nucleus in D_{3h} symmetry.

In methylene, δ values are 0.77 for the $3p_x$ state (in-plane, perpendicular to the symmetry axis), 0.64 for the $3p_y$ state (in-plane, parallel to the symmetry axis), and 0.60 for the $3p_z$ state (perpendicular to the molecular plane).[45] The larger δ for the $3p_x$ state of methylene relative to that of methyl is due to the fact that all the positive charge of the methylene cation core is distributed mainly in the x direction, whereas in methyl, it is spread in the two dimensions of the molecular plane. Note that δ for the $3p_x$ Rydberg state of methylene is almost the same as that in vinyl. The important role of the charge distribution in determining δ values for the in-plane 3p Rydberg states of methylene and methyl is confirmed by the fact that the sum of these δ values is almost the same in both radicals (2.41 in methylene and 2.4 in methyl). Also, this sum for methylene depends only slightly on the H−C−H angle.[45]

Thus, similar to methylene, we explain the large quantum defect for the $3p_x$ Rydberg state of vinyl, which is directed mainly along the C−C bond, by the distribution of the cation core's positive charge along the molecule. In the y direction, the charge distribution in vinyl is similar to that of methyl, and it makes δ for the $3p_y$ Rydberg state of vinyl (0.69) close to δ for the in-plane 3p Rydberg state components of methyl (∼0.7).

There is another effect which may contribute to the large δ for the $3p_x$ state of vinyl. Namely, the center of the charge distribution and, consequently, the nodes of the Rydberg electron wave function no longer coincide with the carbon nuclei, which further increases the probability of finding the Rydberg electron on the carbon nuclei. This is confirmed by the increase of δ for larger αCC angles (up to 0.86 for αCC = 180°), contrary to methylene, in which it changes only slightly upon the increase of the H−C−H angle.[45] This is also confirmed by the increase of the α-C 2s orbital contribution to the Rydberg NBO orbital as the αCC angle increases.

In propen-1-yl or propen-2-yl, as we substitute α- or β-hydrogens with a methyl group, the positive charge distributed along the cation core is more effectively screened by the electrons on the carbon σ bonds. This results in a much smaller penetration of the Rydberg electron into the carbon nuclei, reflected by the large decrease in the quantum defect.

Another interesting observation is a larger decrease in δ relative to vinyl for the $3p_y$ Rydberg state of propen-2-yl compared to propen-1-yl (δ = 0.62 vs 0.67 relative to 0.69 in vinyl). We attribute this difference to the presence of two σ bonds connecting α-C to the other carbons in propen-2-yl versus one in propen-1-yl, which results in a more effective screening of α-C with electrons. Moreover, due to the partial positive charge on the hydrogens, the $3p_y$ Rydberg electron in propen-2-yl tends to move around α-C from which it was removed, which is not the case in propen-1-yl (see Figure 1).

The correlation of the oscillator strengths is shown in Figure 13. Note that the $nl_m \leftarrow n$ transitions are relatively strong. In fact, $3p_y \leftarrow n$ is one of the most intense transitions after the very strong $\pi^* \leftarrow \pi$. The large transition dipole moment for this excitation is due to the large overlap of the singly occupied orbital with the $3p_y$ Rydberg orbital.

The spectral density of the $nl_m \leftarrow n$ Rydberg states increases rapidly with the decrease in IP, as seen in Figures 3−7. For

TABLE 2: Vertical Excitation Energies, Oscillator Strengths, and Properties of the Excited States of the Propen-1-yl Radical[a]

state	transition	ΔE, eV	f_L	μ_{tr}^2, au	$\langle S^2 \rangle$
$^2A''$	$n \leftarrow \pi$	3.04	0.0011	0.0151	0.75
$^4A'$ [b]	$\pi^* \leftarrow \pi$	4.37	0	0	3.75
$^2A''$	$\pi^* \leftarrow n$	5.13	0.0030	0.0241	0.76
$^2A'$ [b]	$\pi^* \leftarrow \pi^d$	5.60	0.0002	0.0014	0.75
$^2A'$	$3s \leftarrow n$	6.14	0.0090	0.0598	0.76
$^2A'$	$3p_y \leftarrow n$	6.77	0.0611	0.3679	0.77
$^2A'$	$3p_x \leftarrow n$	6.92	0.0018	0.0103	0.77
$^4A''$ [c]	$3s \leftarrow \pi$	6.79 (6.82)	0	0	3.75
$^2A''$	$3p_z \leftarrow n$	7.09	0.0166	0.0954	0.96
$^2A''$ [c]	$3s \leftarrow \pi^e$	6.94 (7.12)	0.0187	0.1099	0.74
$^2A''$ [c]	$3s \leftarrow \pi^f$	7.65	0.0005	0.0025	1.10
$^2A'$	$n \leftarrow \sigma_{CC}^-$	7.31	0.0029	0.0165	0.76
$^2A'$	$n \leftarrow \sigma_{CC}^+$	7.47	0.0093	0.0510	0.86
$^4A''$	$3p_x \leftarrow \pi$	7.52	0	0	1.99
$^4A''$	$3p_y \leftarrow \pi$	7.56	0	0	2.01
$^4A'$	$3p_z \leftarrow \pi$	7.57	0	0	1.31
$^2A'$ [b]	$\pi^* \leftarrow \pi^g$	8.15	0.1999	1.0010	1.16

[a] EOM-CCSD/6-311(2+,2+)G(d,p) level of theory using ROHF doublet reference at the geometry from Figure 1 (spherical d-functions, $E_{HF} = -116.451791$ hartree). [b] Calculated by EOM-SF-CCSD with the ROHF $(\pi)^1(\pi^*)^1(n)^1$ quartet reference (spherical d-functions, $E_{HF} = -116.332735$ hartree). [c] Calculated by EOM-SF-CCSD with the ROHF $(\pi)^1(n)^1(3s)^1$ reference (orbitals are optimized for the doublet reference, the 3s orbital is the 16th α-spin orbital by energy in the Hartree−Fock ROHF doublet reference). The EOM-EE-CCSD excitation energy is shown in parentheses. [d] $2(\alpha\pi)(\beta n)(\alpha\pi^*) - (\beta\pi)(\alpha n)(\alpha\pi^*) - (\alpha\pi)(\alpha n)(\beta\pi^*)$. [e] $(\beta\pi)(\alpha n)(\alpha 3s) - (\alpha\pi)(\alpha n)(\beta 3s)$. [f] $2(\alpha\pi)(\beta n)(\alpha 3s) - (\beta\pi)(\alpha n)(\alpha 3s) - (\alpha\pi)(\alpha n)(\beta 3s)$. [g] $(\beta\pi)(\alpha n)(\alpha\pi^*) - (\alpha\pi)(\alpha n)(\beta\pi^*)$.

TABLE 3: Vertical Excitation Energies, Oscillator Strengths, and Properties of the Excited States of the Propen-2-yl Radical[a]

state	transition	ΔE, eV	f_L	μ_{tr}^2, au	$\langle S^2 \rangle$
$^2A''$	$n \leftarrow \pi$	3.29	0.0017	0.0205	0.75
$^4A'$ [b]	$\pi^* \leftarrow \pi$	4.43	0	0	3.75
$^2A''$	$\pi^* \leftarrow n$	4.87	0.0022	0.0186	0.76
$^2A'$ [b]	$\pi^* \leftarrow \pi^d$	5.61	0.0008	0.0062	0.75
$^2A'$	$3s \leftarrow n$	5.70	0.0024	0.0174	0.76
$^2A'$	$3p_y \leftarrow n$	6.39	0.0597	0.3817	0.76
$^2A'$	$3p_x \leftarrow n$	6.45	0.0036	0.0231	0.76
$^2A''$	$3p_z \leftarrow n$	6.66	0.0070	0.0429	0.78
$^4A''$ [c]	$3s \leftarrow \pi$	6.75 (6.80)	0	0	3.75
$^2A''$ [c]	$3s \leftarrow \pi^e$	6.92 (7.01)	0.0225	0.1326	0.73
$^2A''$ [c]	$3s \leftarrow \pi^f$	7.34	0.0026	0.0143	0.76
$^2A'$	$3d_{xy} \leftarrow n$	7.10	0.0034	0.0195	0.76
$^2A'$	$3d_{x^2} \leftarrow n$	7.22	0.0094	0.0532	0.76
$^2A'$	$4s \leftarrow n$	7.29	0.0021	0.0115	0.76
$^2A''$	$3d_{xz} \leftarrow n$	7.36	0.0003	0.0018	0.77
$^2A''$	$3d_{yz} \leftarrow n$	7.42	0.0000	0.0000	0.77
$^2A'$	$n \leftarrow \sigma_{CC}^-$	7.43	0.0250	0.1371	0.79
$^2A'$	$d_{y^2-z^2} \leftarrow n$	7.47	0.0013	0.0071	0.77
$^4A''$	$3p_x \leftarrow \pi$	7.52	0	0	2.01
$^4A''$	$3p_y \leftarrow \pi$	7.58	0	0	1.94
$^4A'$	$3p_z \leftarrow \pi$	7.58	0	0	1.13
$^2A'$	$4p_y \leftarrow n$	7.72	0.0167	0.0884	0.77
$^2A''$	$3p_x \leftarrow \pi$	7.73	0.0043	0.0229	1.66
$^2A'$	$4p_x \leftarrow n$	7.74	0.0012	0.0062	1.05
$^2A'$ [b]	$\pi^* \leftarrow \pi^g$	8.23	0.1886	0.9350	1.29

[a] EOM-CCSD/6-311(2+,2+)G(d,p) level of theory using ROHF doublet reference at the geometry from Figure 1 (spherical d-functions, $E_{HF} = -116.457027$ hartree). [b] Calculated by EOM-SF-CCSD with the ROHF $(\pi)^1(\pi^*)^1(n)^1$ quartet reference (spherical d-functions, $E_{HF} = -116.335488$ hartree). [c] Calculated by EOM-SF-CCSD with the ROHF $(\pi)^1(n)^1(3s)^1$ reference (orbitals are optimized for the doublet reference, the 3s orbital is the 16th α-spin orbital by energy in the Hartree−Fock ROHF doublet reference). The EOM-EE-CCSD excitation energy is shown in parentheses. [d] $2(\alpha\pi)(\beta n)(\alpha\pi^*) - (\beta\pi)(\alpha n)(\alpha\pi^*) - (\alpha\pi)(\alpha n)(\beta\pi^*)$. [e] $(\beta\pi)(\alpha n)(\alpha 3s) - (\alpha\pi)(\alpha n)(\beta 3s)$. [f] $2(\alpha\pi)(\beta n)(\alpha 3s) - (\beta\pi)(\alpha n)(\alpha 3s) - (\alpha\pi)(\alpha n)(\beta 3s)$. [g] $(\beta\pi)(\alpha n)(\alpha\pi^*) - (\alpha\pi)(\alpha n)(\beta\pi^*)$.

example, the $3d \leftarrow n$ states appear at about 7.1 eV in propen-2-yl, but are above 7.5 eV in propen-1-yl. However, the density of Rydberg states in the radicals is even larger due to Rydberg excitations from the π bonding orbital, which appear at relatively low energies.

4. Rydberg $nl_m \leftarrow \pi$ States

Since the $nl_m \leftarrow \pi$ transitions do not involve the half-occupied orbital, they are present in ethylene as well. Similar to the $\pi^* \leftarrow \pi$ transitions (see eq 1 in section 2.6), the coupling of an unpaired electron with the $nl_m \leftarrow \pi$ excitation results in one low-spin quartet and two doublet states:

$$^4\Psi = (\alpha\pi)(\alpha n)(\beta nl_m) + (\alpha\pi)(\beta n)(\alpha nl_m) + (\beta\pi)(\alpha n)(\alpha nl_m)$$

$$^2\Psi_1 = 2(\alpha\pi)(\beta n)(\alpha nl_m) - (\beta\pi)(\alpha n)(\alpha nl_m) - (\alpha\pi)(\alpha n)(\beta nl_m)$$

$$^2\Psi_2 = (\beta\pi)(\alpha n)(\alpha nl_m) - (\alpha\pi)(\alpha n)(\beta nl_m) \qquad (3)$$

and EOM-SF-CCSD should be used instead of EOM-EE-CCSD to reduce spin contamination. In the case of $nl_m \leftarrow \pi$ excitations, however, application of the EOM-SF-CCSD method is problematic because usually Rydberg states can only be described as an excitation to a linear combination of several diffuse Hartree−Fock molecular orbitals. Nevertheless, we attempted EOM-SF-CCSD calculations for the $3s \leftarrow \pi$ states. The "3s" orbital in the high-spin quartet reference $(\pi)(\pi^*)(3s)$ was taken to be the molecular orbital with the largest contribution to the 3s state calculated by the EOM-EE-CCSD method (see section 2.1). As can be seen from Tables 1−5, the difference between the EOM-SF-CCSD and EOM-EE-CCSD excitation energies for the quartet state is less than 0.1 eV, and for the two-configurational doublet it is less than 0.2 eV. Contrary to the $\pi^* \leftarrow \pi$ states, of the two doublets, the two-configurational one is lower in energy. The high excitation energy for the $\pi^* \leftarrow \pi$ two-configurational doublet is due to the Coulomb repulsion between an electron on a π^* orbital and the unpaired electron. In the case of $3s \leftarrow \pi$ transitions, the determining factor is the repulsion between the unpaired electron and an electron on the π orbital rather than the diffuse 3s electron. Since the three-configurational doublet has larger contribution of determinants in which the electrons on the π and n orbitals have opposite spin, the Coulomb electron repulsion in this doublet is higher than that in the two-configurational one. For similar reasons, the excitation energy for the quartet $3s \leftarrow \pi$ state is smaller than that for the corresponding doublets. Thus, one may expect the same behavior for other $nl_m \leftarrow \pi$ Rydberg states.

The changes in the $nl_m \leftarrow \pi$ excitation energies are shown in Figure 14. The IPs for ionization from the π orbital resulting in the triplet cation state of vinyl, propen-1-yl, and propen-2-yl are 10.53, 9.78, and 9.76 eV, respectively. Note that the IPs for ionization resulting in the triplet cation state must be used in eq 2 to estimate excitation energies for the quartet $nl_m \leftarrow \pi$ states. Interestingly, the quantum defect δ for the $3p_x \leftarrow \pi$ quartet state of vinyl is large (0.70) and decreases sharply in propen-1-yl ($\delta = 0.55$) and in propen-2-yl ($\delta = 0.54$), very similar to the $3p_x \leftarrow n$ states (see section 3).

The vertical excitation energies for the triplet $3p_x \leftarrow \pi$, $3p_y \leftarrow \pi$, and $3p_z \leftarrow \pi$ transitions in ethylene are 7.95, 7.94, and 8.21 eV, respectively, and the ionization potential (IP) is 10.56 eV.[46] This gives quantum defect $\delta = 0.72$ for the in-plane 3p

TABLE 4: Vertical Excitation Energies, Oscillator Strengths, and Properties of the Excited States of the *trans*-2-Buten-2-yl Radical[a]

state	transition	ΔE, eV	f_L	μ_{tr}^2, au	$\langle S^2 \rangle$
$^2A''$	$n \leftarrow \pi$	3.02	0.0014	0.0196	0.75
$^4A'$ [b]	$\pi^* \leftarrow \pi$	4.44	0	0	3.75
$^2A''$	$\pi^* \leftarrow n$	5.10	0.0021	0.0170	0.76
$^2A'$ [b]	$\pi^* \leftarrow \pi^d$	5.62	0.0007	0.0050	0.75
$^2A'$	$3s \leftarrow n$	5.64	0.0015	0.0109	0.77
$^2A'$	$3p_y \leftarrow n$	6.14	0.0650	0.4321	0.76
$^2A'$	$3p_x \leftarrow n$	6.26	0.0254	0.1654	0.77
$^2A''$	$3p_z \leftarrow n$	6.38	0.0085	0.0546	0.86
$^4A''$ [c]	$3s \leftarrow \pi$	6.38 (6.44)	0	0	3.75
$^2A''$ [c]	$3s \leftarrow \pi^e$	6.58 (6.63)	0.0068	0.0422	0.76
$^2A''$ [c]	$3s \leftarrow \pi^f$	7.05	0.0004	0.0025	1.05
$^2A'$	$4s \leftarrow n$	6.89	0.0015	0.0088	0.77
$^4A''$	$3p_x \leftarrow \pi$	6.94	0	0	1.97
$^4A''$	$3p_y \leftarrow \pi$	6.99	0	0	1.94
$^2A'$	$3d_{xy} \leftarrow n$	6.99	0.0010	0.0056	0.76
$^2A''$	$3d_{yz} \leftarrow n$	7.01	0.0002	0.0014	0.77
$^2A'$	$3d_{x^2} \leftarrow n$	7.03	0.0036	0.0212	0.77
$^4A'$	$3p_z \leftarrow \pi$	7.06	0	0	1.87
$^2A''$	$3d_{xz} \leftarrow n$	7.15	0.0001	0.0006	0.78
$^2A''$	$3p_x \leftarrow \pi$	7.19	0.0000	0.0001	1.74
$^2A'$	$n \leftarrow \sigma_{CC}$	7.20	0.0012	0.0065	0.86
$^2A'$	$3d_{y^2-z^2} \leftarrow n$	7.29	0.0012	0.0068	0.85
$^2A'$ [b]	$\pi^* \leftarrow \pi^g$	8.38	0.4053	1.9747	1.04

[a] EOM-CCSD/6-311(2+,2+)G(d,p) level of theory using ROHF doublet reference at the geometry from Figure 1 (spherical d-functions, $E_{HF} = -155.504207$ hartree). [b] Calculated by EOM-SF-CCSD with the ROHF $(\pi)^1(\pi^*)^1(n)^1$ quartet reference (spherical d-functions, $E_{HF} = -155.380248$ hartree). [c] Calculated by EOM-SF-CCSD with the ROHF $(\pi)^1(n)^1(3s)^1$ reference (orbitals are optimized for the doublet reference, the 3s orbital is the 26th α-spin orbital by energy in the Hartree−Fock ROHF doublet reference). The EOM-EE-CCSD excitation energy is shown in parentheses. [d] $2(\alpha\pi)(\beta n)(\alpha\pi^*) - (\beta\pi)(\alpha n)(\alpha\pi^*) - (\alpha\pi)(\alpha n)(\beta\pi^*)$. [e] $(\beta\pi)(\alpha n)(\alpha 3s) - (\alpha\pi)(\alpha n)(\beta 3s)$. [f] $2(\alpha\pi)(\beta n)(\alpha 3s) - (\beta\pi)(\alpha n)(\alpha 3s) - (\alpha\pi)(\alpha n)(\beta 3s)$. [g] $(\beta\pi)(\alpha n)(\alpha\pi^*) - (\alpha\pi)(\alpha n)(\beta\pi^*)$.

components, which is almost the same as δ for the in-plane 3p components of the methyl radical. This indicates similar cation core positive charge distributions in ethylene and methyl. The calculated quartet $3p_x \leftarrow \pi$ excitation energy for vinyl is the same as the triplet $3p_x \leftarrow \pi$ excitation energy for ethylene (7.95 eV). Also, the IP for the ionization of vinyl resulting in the triplet cation state, 10.53 eV, is very close to the IP of ethylene, 10.56 eV. However, the IP for the ionization resulting in the singlet cation state of vinyl is higher, 11.30 eV. The reason for the higher-multiplicity cation and the $3p_x \leftarrow \pi$ excited state of vinyl being similar to those of ethylene is also the reduced Coulomb repulsion between an electron on the half-filled orbital and the remaining electron on the π bonding orbital. Note that, although this reduction in the Coulomb repulsion lowers the quartet $3p_x \leftarrow \pi$ state of vinyl relative to the corresponding doublets, the penetration of the Rydberg electron to the cation core ($\delta = 0.70$) is less than that in the case of the $3p_x \leftarrow n$ excitation ($\delta = 0.76$).

5. Conclusions

We presented the results of high-level ab initio calculations of the ground and first excited state equilibrium geometries, vertical excitation energies, oscillator strengths, and valence states' permanent dipole moments for the vinyl, propen-1-yl, propen-2-yl, 1-buten-2-yl, and *trans*-2-buten-2-yl radicals. The electronic spectrum of these species is very dense and is dominated by Rydberg transitions. The electronic structure and energetics of the valence low-lying excited states are similar in all the radicals, except for the $n \leftarrow \sigma$ states, which change

TABLE 5: Vertical Excitation Energies, Oscillator Strengths, and Properties of the Excited States of the 1-Buten-2-yl Radical[a]

state	transition	ΔE, eV	f_L	μ_{tr}^2, au
^2A	$n \leftarrow \pi$	3.28	0.0014	0.0216
^4A [b]	$\pi^* \leftarrow \pi$	4.42	0	0
^2A	$\pi^* \leftarrow n$	4.81	0.0026	0.0216
^2A [b]	$\pi^* \leftarrow \pi^d$	5.58	0.0008	0.0055
^2A	$3s \leftarrow n$	5.73	0.0024	0.0173
^2A	$3p_y \leftarrow n$	6.27	0.0616	0.4014
^2A	$3p_x \leftarrow n$	6.40	0.0054	0.0346
^2A	$3p_z \leftarrow n$	6.52	0.0081	0.0505
^4A [c]	$3s \leftarrow \pi$	6.78 (6.83)	0	0
^2A [c]	$3s \leftarrow \pi^e$	6.94	0.0300	0.1764
^2A [c]	$3s \leftarrow \pi^f$	7.35	0.0056	0.0309
^2A	$n \leftarrow \sigma_{CC}$, $3s \leftarrow \pi$	7.03	0.0199	0.1157
^2A	$n \leftarrow \sigma_{CC}$	7.04	0.0111	0.0645
^2A	$4s \leftarrow n$	7.05	0.0038	0.0218
^2A	$3d \leftarrow n$	7.10	0.0025	0.0147
^2A	$3d \leftarrow n$	7.18	0.0021	0.0121
^2A	$3d \leftarrow n$	7.23	0.0003	0.0015
^2A	$3d \leftarrow n$	7.26	0.0004	0.0023
^2A	$3d \leftarrow n$	7.42	0.0068	0.0372
^4A	$3p_z \leftarrow \pi$	7.45	0.0777	0.4257
^4A	$3p_y \leftarrow \pi$	7.48	0.0013	0.0073
^4A	$3p_x \leftarrow \pi$	7.57	0	0
^2A	$4p_y \leftarrow n$	7.58	0.0109	0.0585
^2A	$4p_x \leftarrow n$	7.61	0.0033	0.0176
^2A	$3p_x \leftarrow \pi$	7.63	0.0502	0.2684
^2A	$3p_y \leftarrow \pi$	7.67	0.0032	0.0170
^2A	$4p_z \leftarrow n$	7.71	0.0011	0.0057
^2A	$3p_x \leftarrow \pi$	7.77	0.0062	0.0328
^2A [b]	$\pi^* \leftarrow \pi^g$	8.04	0.2395	1.2163

[a] EOM-CCSD/6-311(2+,2+)G(d,p) level of theory using ROHF doublet reference at the geometry from Figure 1 (spherical d-functions, $E_{HF} = -155.500917$ hartree). [b] Calculated by EOM-SF-CCSD with the ROHF $(\pi)^1(\pi^*)^1(n)^1$ quartet reference (spherical d-functions, $E_{HF} = -155.379309$ hartree). [c] Calculated by EOM-SF-CCSD with the ROHF $(\pi)^1(n)^1(3s)^1$ reference (orbitals are optimized for the doublet reference, the 3s orbital is the 17th α-spin orbital by energy in the Hartree−Fock ROHF doublet reference). The EOM-EE-CCSD excitation energy is shown in parentheses. [d] $2(\alpha\pi)(\beta n)(\alpha\pi^*) - (\beta\pi)(\alpha n)(\alpha\pi^*) - (\alpha\pi)(\alpha n)(\beta\pi^*)$. [e] $(\beta\pi)(\alpha n)(\alpha 3s) - (\alpha\pi)(\alpha n)(\beta 3s)$. [f] $2(\alpha\pi)(\beta n)(\alpha 3s) - (\beta\pi)(\alpha n)(\alpha 3s) - (\alpha\pi)(\alpha n)(\beta 3)$. [g] $(\beta\pi)(\alpha n)(\alpha\pi^*) - (\alpha\pi)(\alpha n)(\beta\pi^*)$.

substantially with the number of adjacent σ bonds. The excitation energies for the Rydberg states, however, depend strongly on the size and the structure of the radicals. The major factor responsible for the changes in the Rydberg states' energies is the strong dependence of the ionization potentials on the size and geometric structure. Our results suggest that the quantum defect δ for the $3p_x$, $3p_y$, and $3p_z$ Rydberg states is determined by the geometry-dependent charge distribution within the cation core.

We interpret the elongation of the in-plane C−H bonds in the ground state propen-1-yl, propen-2-yl, and *trans*-2-buten-2-yl radicals as an indication of the hyperconjugative charge transfer from the in-plane C−H bonds to the half-filled orbital. This is consistent with the orientation of the ethyl group in 1-buten-2-yl, in which one of the C−H bonds is also elongated and is almost in one plane with the half-filled orbital.

On the basis of the results of accurate ab initio calculations, we derived the qualitative picture encompassing the effects of substitution of hydrogens with methyl or ethyl groups in unsaturated hydrocarbons. We hope that this qualitative understanding will be useful in prediction of excited state properties and reaction pathways of these and similar species.

Acknowledgment. We would like to thank Professor Laurie J. Butler and her group for drawing our interest to the fascinating

area of unsaturated hydrocarbon radicals and providing us with useful insights regarding the details of their experiment. This work was supported by the Department of Energy (DE-FG02-05ER15685), the National Science Foundation (CAREER Award CHE-0094116), Alfred P. Sloan Foundation, and the WISE Research Fund (USC).

References and Notes

(1) Shimamura, O. *Topics in Stereochemistry*; Wiley: New York, 1969.
(2) Okabe, H. *Photochemistry of Small Molecules*; Wiley: New York, 1978.
(3) Gardiner, W. C., Ed. *Gas-Phase Combustion Chemistry*; Springer: New York, 2000.
(4) Fensterbank, L.; Malacria, M.; Sieburth, S. M. *Synthesis* **1997**, 813.
(5) Kanamori, H.; Endo, Y.; Hirota, E. *J. Chem. Phys.* **1990**, *92*, 197.
(6) Hunziker, H. E.; Kneppe, H.; McLean, A. D.; Siegbahn, P.; Wendt, H. R. *Can. J. Chem.* **1983**, *61*, 993.
(7) Pibel, C. D.; Mcllroy, A.; Taatjes, C. A.; Alfred, S.; Patrick, K.; Halpern, J. B. *J. Chem. Phys.* **1998**, *110*, 1841.
(8) Shahu, M.; Yang, C.-H.; Pibel, C. D.; Mcllroy, A.; Taatjes, C. A.; Halpern, J. B. *J. Chem. Phys.* **2002**, *116*, 8343.
(9) Pushkarsky, M. B.; Mann, A. M.; Yeston, J. S.; Moore, C. B. *J. Chem. Phys.* **2001**, *115*, 10738.
(10) Fahr, A.; Laufer, A. H. *J. Phys. Chem.* **1988**, *92*, 7229.
(11) Fahr, A.; Hassanzadeh, P.; Atkinson, D. B. *Chem. Phys.* **1998**, *236*, 43.
(12) Miller, J. L.; Krisch, M. J.; Butler, L. J. *J. Phys. Chem. A* **2005**, *109*, 4038.
(13) McCunn, L. R.; Krisch, M. J.; Liu, Y.; Butler, L. J.; Shu, J. *J. Phys. Chem. A* **2005**, *109*, 6430.
(14) Sevin, A.; Yu, H. T.; Evleth, E. M. *J. Mol. Struct. (THEOCHEM)* **1983**, *104*, 163.
(15) Paddon-Row, M. N.; Pople, J. A. *J. Phys. Chem.* **1985**, *89*, 2768.
(16) Wang, J.-H.; Chang, H.-C.; Chen, Y.-T. *Chem. Phys.* **1996**, *206*, 43.
(17) Mebel, A. M.; Chen, Y.-T.; Lin, S.-H. *Chem. Phys. Lett.* **1997**, *275*, 19.
(18) Zhang, P.; Morokuma, K. *Chem. Phys. Lett.* **2003**, *367*, 482.
(19) Zhang, P.; Irle, S.; Morokuma, K.; Tschumper, G. S. *J. Chem. Phys.* **2003**, *119*, 6524.
(20) Peterson, K. A.; Dunning, T. H., Jr. *J. Chem. Phys.* **1997**, *106*, 4119.
(21) Raghavachari, K.; Trucks, G. W.; Pople, J. A.; Head-Gordon, M. *Chem. Phys. Lett.* **1989**, *157*, 479.
(22) Watts, J. D.; Gauss, J.; Bartlett, R. J. *J. Chem. Phys.* **1993**, *98*, 8718.
(23) Stanton, J. F.; Gauss, J.; Watts, J. D.; Lauderdale, W. J.; Bartlett, R. J. *ACES II*, 1993. The package also contains modified versions of the MOLECULE Gaussian integral program of J. Almlöf and P. R. Taylor, the ABACUS integral derivative program written by T. U. Helgaker, H. J. Aa. Jensen, P. Jørgensen, and P. R. Taylor, and the PROPS property evaluation integral code of P. R. Taylor.
(24) Krishnan, R.; Binkley, J. S.; Seeger, R.; Pople, J. A. *J. Chem. Phys.* **1980**, *72*, 650.
(25) McLean, A. D.; Chandler, G. S. *J. Chem. Phys.* **1980**, *72*, 5639.
(26) Koch, H.; Jensen, H. J. Aa.; Jørgensen, P.; Helgaker, T. *J. Chem. Phys.* **1990**, *93*, 3345.
(27) Stanton, J. F.; Bartlett, R. J. *J. Chem. Phys.* **1993**, *98*, 7029.
(28) Levchenko, S. V.; Krylov, A. I. *J. Chem. Phys.* **2004**, *120*, 175.
(29) Sinha, D.; Mukhopadhyay, D.; Mukherjee, D. *Chem. Phys. Lett.* **1986**, *129*, 369.
(30) Sinha, D.; Mukhopadhya, D.; Chaudhuri, R.; Mukherjee, D. *Chem. Phys. Lett.* **1989**, *154*, 544.
(31) Chaudhuri, R.; Mukhopadhyay, D.; Mukherjee, D. *Chem. Phys. Lett.* **1989**, *162*, 393.
(32) Kong, J.; White, C. A.; Krylov, A. I.; Sherrill, C. D.; Adamson, R. D.; Furlani, T. R.; Lee, M. S.; Lee, A. M.; Gwaltney, S. R.; Adams, T. R.; Ochsenfeld, C.; Gilbert, A. T. B.; Kedziora, G. S.; Rassolov, V. A.; Maurice, D. R.; Nair, N.; Shao, Y.; Besley, N. A.; Maslen, P.; Dombroski, J. P.; Daschel, H.; Zhang, W.; Korambath, P. P.; Baker, J.; Bird, E. F. C.; Van Voorhis, T.; Oumi, M.; Hirata, S.; Hsu, C.-P.; Ishikawa, N.; Florian, J.; Warshel, A.; Johnson, B. G.; Gill, P. M. W.; Head-Gordon, M.; Pople, J. A. *J. Comput. Chem.* **2000**, *21*, 1532.
(33) Kundu, T.; Pradhan, B.; Singh, B. P. *Proc. Ind. Acad. Sci. (Chem. Sci.)* **2002**, *114*, 623.
(34) Prophristic, V.; Goodman, L. *Nature* **2001**, *411*, 565.
(35) Brunck, T. K.; Weinhold, F. *J. Am. Chem. Soc.* **1979**, *101*, 1700.
(36) Ingold, K. U.; Wright, J. S. *J. Chem. Educ.* **2000**, *77*, 1062.
(37) Larsen, H.; Hald, K.; Olsen, J.; Jørgensen, P. *J. Chem. Phys.* **2001**, *115*, 3015.
(38) Helgaker, T.; Jørgensen, P.; Olsen, J. *Molecular Electronic Structure Theory*; John Wiley & Sons: New York, 2000.
(39) Ethylene vertical excitation energies were calculated using EOM-EE-CCSD/6-311(2+,2+)G(d,p) at the geometry from Saxe et al. *J. Chem. Phys.* **1982**, *77*, 5584 (r_{CH} = 1.076 Å, ∠HCC = 121.7°, D_{4h} symmetry).
(40) Szalay, P. G.; Gauss, J. *J. Chem. Phys.* **2000**, *112*, 4027.
(41) Mulliken, R. S. *J. Chem. Phys.* **1939**, *7*, 20.
(42) Herzberg, G. *Molecular Spectroscopy and Molecular Structure: Electronic Spectra end Electronic Structure of Polyatomic Molecules*; van Nostrand Reinhold: New York, 1966; Vol. III.
(43) Glendening, E. D.; Badenhoop, J. K.; Reed, A. E.; Carpenter, J. E.; Bohmann, J. A.; Morales, C. M.; Weinhold, F. *NBO 5.0*; Theoretical Chemistry Institute, University of Wisconsin: Madison, WI, 2001.
(44) Martín, I.; Velasco, A. M.; Lavín, C. *Int. J. Quantum Chem.* **2002**, *86*, 59.
(45) The excitation energies and IPs for the 3p Rydberg states of methylene were calculated using the EOM-EE-CCSD and EOM-IP-CCSD methods, respectively, with the 6-311(2+,2+)G** basis set (spherical d-functions) and the triplet ROHF reference. We considered only the 3p Rydberg states corresponding to excitation from the out-of-plane half-filled orbital. We used the following geometry: r_{CH} = 1.077 Å, ∠HCH = 134° (C_{2v} symmetry). We also calculated the quantum defects at the geometries with one or both r_{CH} = 1.096 Å and found that the quantum defects are insensitive to the C−H bond lengths. At ∠HCH = 90° and r_{CH} = 1.077 Å, the quantum defects were found to be 0.72 for the $3p_x$ state, 0.69 for the $3p_y$ state, and 0.62 for the $3p_z$ state, and the sum of δ values for the in-plane Rydberg states is 2.41. At ∠HCH = 179°, the quantum defects were found to be 0.78 for the $3p_x$ state and 0.64 for the $3p_{y,z}$ states. Once again, the sum of δ values for the $3p_x$ and $3p_y$ components, 2.42, is very close to the sum at the other geometries.
(46) The vertical excitation energies for the 3p ← π transitions in ethylene were calculated at the EOM-EE-CCSD/6-311(2+,2+)G** level of theory (spherical functions were used). The orientation of the molecule was as follows: the carbon atoms are on the *x* axis, *xy* is the plane of the molecule, and the *z* axis is perpendicular to the plane. The ionization potential was calculated at the EOM-IP-CCSD/6-311(2+,2+)G** level of theory.